Applied Thermal Engineering 110 (2017) 795–804

Contents lists available at ScienceDirect

Applied Thermal Engineering

journal homepage: www.elsevier.com/locate/apthermeng

Research Paper

Improvement of fuel oil spray combustion inside a 7 MW industrial furnace: A numerical study

Igor Bonefačić, Igor Wolf, Paolo Blecich *

Faculty of Engineering, University of Rijeka, Vukovarska 58, 51000 Rijeka, Croatia

HIGHLIGHTS

- Small spray angles cause delayed fuel ignition, which increases species emissions.
- Moderate swirl numbers reduce species emissions and increase the heating output.
- Large swirl numbers or spray angles speed up fuel ignition but shorten the flames.
- Excessive flame shortening reduces species emissions but also the heating output.

ARTICLE INFO

Article history:
Received 23 March 2016
Revised 30 August 2016
Accepted 31 August 2016
Available online 2 September 2016

Keywords:
Numerical analysis
Spray combustion
Air-fuel ratio
Swirl number
Spray angle
Droplet diameter

ABSTRACT

This paper presents a numerical analysis of fuel oil spray combustion inside an industrial furnace. The industrial furnace is a 7 MW cylindrical furnace which supplies heat to an oil refinery. The commercial CFD software Fluent is used for modeling transport and reaction processes in the furnace. The chosen combustion model is validated against measurement data available in the literature and good agreement is achieved. Fuel oil spray combustion is improved by varying fuel and burner parameters such as relative air-fuel ratio, fuel droplet diameter, fuel spray half-angle and burner swirl number. These parameters affect the flame shape and stability, on which depends the performance of the industrial furnace, particularly the heating output and gas species emissions. The numerical analysis revealed that complete combustion and minimum fractions of unburnt species are obtained by lean air-fuel mixtures, highly swirling flows, wide fuel spray angles and small fuel droplets. On the other side, the highest furnace heating outputs are achieved for near-stoichiometric air-fuel mixtures, narrow fuel spray angles, swirl numbers between 0.6 and 1.0 and small fuel droplets.

1. Introduction

With a share of 80% at global scale, fossil fuels are still the major source of energy despite growing concerns about climate change, energy prices and supply security [1]. Fossil fuels are burned in power plants to generate electricity, in vehicles, ships and airplanes to generate mechanical work, or in buildings to supply heating energy. Fossil fuels are converted into energy with combustion processes that generate useful heat but also harmful flue gases. Consequently, the combustion process of fossil fuels is still a frequently addressed field of research. The analysis of combustion processes was confined to measurements and observations prior to the development of computer simulation software. Nowadays, computer simulation is indispensable for the analysis and advancement of combustion processes with pulverized coal [2], gaseous fuels [3,4] or liquid fuel sprays [5–7]. Computer simulations of the physical and chemical processes during liquid fuel combustion include numerical solutions of multidimensional, steady or transient, differential equations for the conservation of mass, momentum and energy. A number of sub-models are coupled within the procedure: turbulence-chemistry interaction, heat and mass interaction between discrete and continuous phase, radiative heat transfer, NOx, SOx and soot formation. Advances in theory and simulation of dispersion, transport, evaporation and combustion of liquid fuel sprays are presented in the review papers [7–9].

Jenny et al. [7] provide a comprehensive review of computational models relevant for turbulent dilute spray combustion. They analyze the properties of the general modeling approaches and combustion models and report the current understanding of various physical phenomena encountered in turbulent spray

* Corresponding author.
E-mail address: paolo.blecich@riteh.hr (P. Blecich).

http://dx.doi.org/10.1016/j.applthermaleng.2016.08.218
1359-4311/

combustion. The authors conclude that further work is necessary for the development and experimental validation of computer models for droplet collision, breakup, dispersion and mixing.

Chiu [8] reviews the major theoretical accomplishments in droplet and spray combustion. The author examines the major analytical developments and critical bottlenecks in the theory of droplet physics. He also discusses the recent findings and future prospects of a unified theory of droplet phenomena.

Sirignano [9] comments the recent advances in droplet array vaporization and combustion theory and computer modeling. The author deepens the subject with the newest understandings in the field of transient convective combustion of droplet arrays, including extensions to non-unitary Lewis number and multicomponent liquid fuels. Special attention is given to the effects of droplet deceleration due to drag, droplet diameter reduction due to vaporization and internal liquid circulation.

Experimental and numerical studies of fuel oil spray combustion are presented in [10–13]. Saario et al. [10] concluded that the standard k-ε (SKE) turbulence model cannot predict faithfully the highly swirling flow field and that the Reynolds stress model (RSM) should be used instead. They conclude that the RSM model is capable of producing reasonably good predictions for O_2, CO_2, CO and NO concentrations, except in the near burner region. Barreiros et al. [11] found that the burner geometry and air inlet velocity have strong influence on gas temperatures, gas velocities and species concentration in the furnace. They reported NOx concentrations as function of burner swirl number and concluded that fast droplet evaporation and long residence time contribute NOx reduction. Ling et al. [12] achieved lower NOx and CO concentrations with a combustion configuration that consists of swirl burners with Y-type atomizing nozzles and air staging, overfire air and flue gases recirculation. Wu et al. [13] investigated the effect of the number and type of atomizers, as well as their firing mode and location in industrial burners on NO emissions for fuel oil spray combustion. They concluded that double-mixed-vortex atomizers with single direct fuel injection firing mode reduce NO emissions.

The above cited papers focused mostly on the effects of burner geometry on NOx concentrations. This paper extends the numerical analysis on other parameters affecting fuel oil spray combustion, such as the air-fuel ratio, fuel oil droplet diameter, fuel spray half-angle and burner swirl number. The aim is to improve the performance of a cylindrical industrial furnace, which supplies heat to the refinery process of oil vacuum distillation. The commercial CFD software Fluent 6.3 is employed for this purpose. Measurement data from inside the combustion chamber of the industrial furnace does not exist and probing was not possible. Nevertheless, the chosen combustion model is validated against measurements found in the literature [10]. These measurements include CO_2, O_2 and NO fractions for several positions inside a down-fired laboratory furnace.

2. Mathematical model

2.1. Fuel oil spray combustion model

Fuel oil spray combustion in the cylindrical industrial furnace is modeled using the non-premixed approach. In non-premixed combustion, fuel and air enter the flame region separately, mix, react and produce combustion gases. The thermochemical state of the gases is assumed to be related to the mixture fraction, Z, which represents the local concentration of fuel or oxygen and is defined as

$$Z = \frac{sY_F - (Y_{O_2} - Y_{O_2,in})}{sY_{F,in} + Y_{O_2,in}}; \quad s = \frac{W_{O_2}\nu_{O_2}}{W_F\nu_F} \tag{1}$$

The local fuel and oxygen mass fractions are Y_F and Y_{O2}, and the inlet stream mass fractions are $Y_{F,in}$ and $Y_{O2,in}$. The stoichiometric oxygen to fuel mass ratio is denoted with s, the species molecular weights are W_{O2} and W_F, and the stoichiometric coefficients ν_{O2} and ν_F. The probability of mixture fraction having a value of Z is predicted by a presumed probability distribution function (PDF). The Beta distribution [14] gives good predictions of the mixture fraction probability since it closely resembles the experimentally observed PDFs. The conserved quantities ϕ_i such as species fractions, mean temperature and density are derived from the predicted mixture fraction field

$$\phi_i = \phi_i(Z) \tag{2}$$

The mixture fraction approach is convenient for modeling turbulent reactive flows where turbulent convection dominates over molecular diffusion, that is, where reactions occur much faster than mixing. Also, the following assumptions should be met: turbulent flow, fast reaction rate chemistry, equal thermal and mass diffusivity, and discrete fuel and oxidizer inlets. Since the gas density varies in reacting flows, the instantaneous value of a conserved quantity, ϕ_i, is expressed by the Favre-averaged (density-weighted) component, $\tilde{\phi}_i$, and the fluctuating component ϕ_i''

$$\phi_i = \tilde{\phi}_i + \phi_i'' = \overline{\rho\phi_i}/\bar{\rho} + \phi_i'' \tag{3}$$

Turbulent reacting flows are modeled with a set of Favre-averaged conservation equations:

$$\text{continuity}: \quad \frac{\partial\bar{\rho}}{\partial t} + \frac{\partial(\bar{\rho}\tilde{w}_j)}{\partial x_j} = 0 \tag{4}$$

$$\text{momentum}: \quad \frac{\partial(\bar{\rho}\tilde{w}_i)}{\partial t} + \frac{\partial(\bar{\rho}\tilde{w}_i\tilde{w}_j)}{\partial x_j} = -\frac{\partial\bar{p}}{\partial x_i} + \frac{\partial}{\partial x_j}\left(\bar{\tau}_{ij} - \overline{\rho w_i'' w_j''}\right) \tag{5}$$

$$\text{energy}: \quad \frac{\partial(\bar{\rho}\tilde{h})}{\partial t} + \frac{\partial(\bar{\rho}\tilde{w}_j\tilde{h})}{\partial x_j} = \frac{\partial}{\partial x_j}\left(\Gamma_h\frac{\partial\tilde{h}}{\partial x_j}\right) \tag{6}$$

$$\text{mixture fraction}: \quad \frac{\partial(\bar{\rho}\tilde{Z})}{\partial t} + \frac{\partial(\bar{\rho}\tilde{w}_j\tilde{Z})}{\partial x_j} = \frac{\partial}{\partial x_j}\left(\Gamma_Z\frac{\partial\tilde{Z}}{\partial x_j}\right) \tag{7}$$

The transport equations for gas species are included in the mixture fraction Eq. (7). Species fractions are derived from the mixture fraction using semiempirical state relationships. A total of 20 species are determined from equilibrium calculations. Fuel oil constituents are C, H, S and N while air constituents are N_2 and O_2. The most dominant product species are N_2, CO_2, H_2O and O_2, while CO and H_2 have smaller fractions. Intermediate species such as CH_4, C_2H_2, C_2H_4, C_4H_2 and C_6H_6 are also created. NOx and SOx species are excluded from equilibrium calculations since they have low concentrations and negligible impact on density, temperature and other species. However, NOx and SOx can be predicted from the solution of the flow field, using the Fluent post-processing tools.

2.2. Discrete particle model

Fuel oil droplets in the gas phase are described by the following set of conservation equations

$$\text{mass}: \quad \frac{dm_p}{dt} = -G_p \tag{8}$$

$$\text{momentum}: \quad \frac{dw_p}{dt} = F_p(w - w_p) + \frac{g_x(\rho_p - \rho)}{\rho_p} + F_x \tag{9}$$

$$\text{energy}: m_p c_p \frac{dT_p}{dt} = \sum Q_p \tag{10}$$

In the mass conservation Eq. (8), the fuel oil droplet mass m_p, changes by the rate of vaporization G_p. The momentum conservation Eq. (9) balances the droplet inertia with the forces arising due to drag, gravity and pressure gradients in the gas phase. The dispersion of droplets is predicted using the stochastic tracking model (discrete random walk). Here, the average particle trajectory in the gas phase is computed from a number of representative particles. Heat and mass transfer between fuel oil droplets and gas phase is solved by three laws. The inert heating law applies on droplets having temperatures below the vaporization temperature

$$m_p c_p \frac{dT_p}{dt} = hA_p(T_\infty - T_p) + \varepsilon_p A_p \sigma(T_R^4 - T_p^4) \tag{11}$$

In Eq. (11), the fuel droplet has a temperature of T_p, a surface area of A_p, an emissivity of ε_p and a heat capacity of c_p, the radiation temperature is T_R and the continuous phase temperature is T_∞. When the droplet temperature is in the range between the vaporization (400 K) and the boiling temperature (589 K), Eq. (11) is expanded by the term for latent heat transfer and forms the vaporization law

$$m_p c_p \frac{dT_p}{dt} = hA_p(T_\infty - T_p) + r\frac{dm_p}{dt} + \varepsilon_p A_p \sigma(T_R^4 - T_p^4) \tag{12}$$

During droplet vaporization, the droplet mass reduction (i.e. the rate of vaporization) over a discrete time step Δt is calculated from the gradient of vapor concentration between the droplet surface and in the gas phase

$$m_p(t + \Delta t) - m_p(t) = -\kappa(C_{i,s} - C_{i,\infty})A_p M_i \Delta t \tag{13}$$

The vapor concentration at the droplet surface $C_{i,s}$ and in the gas phase $C_{i,\infty}$ is calculated using the Dalton's law of partial pressures

$$C_{i,s} = \frac{p_{sat}}{RT_p}, \quad C_{i,\infty} = \frac{X_i p}{RT_\infty} \tag{14}$$

In (14) it is assumed that the vapor pressure at the droplet surface is equal to the saturated vapor pressure p_{sat} at the droplet temperature T_p. The vapor pressure in the gas phase is calculated from the local fuel mole fraction X_i and the local absolute pressure of the gas phase. The universal gas constant is denoted with R and the fuel molecular weight with M_i. The heat and mass transfer coefficients, h and κ, are calculated using the Ranz-Marshall [15] heat and mass transfer analogy

$$Nu = hd_p/k_\infty = 2 + 0.6Re_p^{0.5}Pr^{0.33} \tag{15}$$

$$Sh = \kappa d_p/D_{i,\infty} = 2 + 0.6Re_p^{0.5}Sc^{0.33} \tag{16}$$

The droplet Reynolds number Re_p is based on the droplet relative velocity $|w_p - w_\infty|$, the droplet diameter d_p and on the viscosity of the gas phase v

$$Re_d = |w_p - w_\infty| \cdot d_p/v \tag{17}$$

When the droplet temperature is equal to or higher than the boiling point temperature, the rate of vaporization is calculated from the boiling law

$$-r\frac{dm_p}{dt} = hA_p(T_\infty - T_p) + \varepsilon_p A_p \sigma(T_R^4 - T_p^4) \tag{18}$$

Complete evaporation of fuel oil droplets is assumed, that is no coke particles are formed after burnout. Coalescence and break-up of oil droplets are neglected.

2.3. Turbulence model

Three turbulence models are considered. The standard k-ε (SKE) turbulence model is the most widely used, but its major shortcoming is the assumption of isotropic turbulence. This limitation may seriously affect the results in highly swirling flows. The realizable k-ε (RKE) turbulence model offers improved accuracy for rotating flows involving separation and recirculation [16]. For low-swirl flows ($S < 0.5$) the RKE model ensures appreciable improvements over the SKE model, while for high-swirl flows ($S > 0.5$), the Reynolds stress model (RSM) is recommended [16]. The RSM model solves directly the stress terms of momentum equations and produce better results than k-ε based models in highly swirling non-isotropic turbulent flows. In Section 3, the results of the three turbulence models are compared against measurements for species fractions found in the literature. The linkage between continuity and momentum equations is performed by the SIMPLE algorithm.

2.4. Heat radiation model

Radiative heat transfer in the furnace is solved using the discrete ordinates (DO) heat radiation model. Both the gas phase and particles influence heat radiation from the flame. The weighted sum-of-grey-gases (WSGGM) model is used to determine the absorption coefficient of the gas phase. The effect of particles on the absorption coefficient is taken into account enabling the particle radiation interaction option in Fluent. The overall absorption coefficient is defined as the sum of the absorption coefficients of the gas phase and soot. Soot generation is modeled using the two-step Tesner model [17] that predicts the generation of nuclei on which soot is generated. The transport equations for soot fractions and nuclei concentrations have the form of the general species transport Eq. (22). The source terms include the rates of soot and nuclei generation, S_{soot} and S_{nuc}, respectively. The rate of soot generation S_{soot} is calculated as the difference between the rate of soot formation [17] and the rate of soot combustion [18], that is

$$S_{soot} = S_{soot,form} - S_{soot,comb} \tag{19}$$

The rate of soot formation, $S_{soot,form}$ depends on the nuclei concentration

$$S_{soot,form} = m_{p,soot}(a + bC_{soot})C_{nuc} \tag{20}$$

where $m_{p,soot}$ is the mean mass of the soot particle, C_{soot} and C_{nuc} are soot particles and nuclei particles concentrations, respectively, a and b are empirical constants. The Magnussen model [18] choses the rate of the soot combustion as the smaller value from two combustion rates, that is

$$S_{soot,comb} = \min\left[\left(A\rho Y_{soot}\frac{\varepsilon}{k}\right), \left(A\rho\frac{Y_{O_2}Y_{soot}}{Y_{soot}v_{soot} + Y_F v_F}\frac{\varepsilon}{k}\right)\right] \tag{21}$$

where Y_{soot}, Y_{O2} and Y_F are the local soot, oxygen and fuel mass fractions, A is a model constant, k and ε are the turbulent kinetic energy and its dissipation rate, v_{soot} and v_F are the stoichiometric coefficients for soot and fuel. The rate of nuclei generation S_{nuc} is modeled similarly to the rate of soot generation, as the difference between nuclei formation rate and nuclei combustion rate [17].

2.5. NOx and SOx model

NOx and SOx emissions are predicted from the flow field solution, using the Fluent post-processing tools. The NOx model includes nitric oxide (NO) while nitrogen dioxide (NO_2) and nitrous oxide (N_2O) are neglected. The NO formation model takes into account reactions for thermal, fuel and prompt NO. Thermal NO is modeled by the extended Zeldovich mechanism [19]. Fuel NO formation is modeled assuming that all fuel nitrogen converts into hydrogen cyanide (HCN).

SOx emissions, which consist sulfur dioxide (SO_2) and sulfur trioxide (SO_3), are modeled with an eight-step reduced mechanism

[20]. For liquid fuels, it can be assumed that all fuel-bound sulfur is released as hydrogen sulfide (H_2S). For sulfur reacting with the gas phase, the intermediate sulfur monoxide (SO) and hydrosulfide radical (SH) are included in the SOx model. The transport equations for concentrations of NOx and SOx species follow the general species transport equation

$$\frac{\partial(\bar{\rho}\widetilde{Y}_i)}{\partial t}+\frac{\partial\left(\bar{\rho}\tilde{w}_j\widetilde{Y}_i\right)}{\partial x_j}=\frac{\partial}{\partial x_j}\left(\Gamma_i\frac{\partial\widetilde{Y}_i}{\partial x_j}\right)+S_i \tag{22}$$

3. Computational model

3.1. The industrial furnace

The industrial furnace is a cylindrical, vertically-fired furnace that supplies heat for the process of vacuum distillation in the oil refinery of the City of Rijeka (Croatia). The furnace is 15 m in height and consists of four main parts: the furnace base with three burners, the radiant section, the conical convection section and the chimney, as shown in Fig. 1. The radiant section is 7 m in height and 2.8 m in diameter. The radiant section is followed by a conical section and the chimney. The conical section is 2 m in height and directs flue gases into the chimney duct which is 6 m in height and 0.8 m in diameter. The furnace burns heavy fuel oil. Taking into account that the fuel consumption is 837 kg/h and that its lower heating value is 40.68 MJ/kg, the heat content of the fuel is 9.45 MW. The refinery states that the industrial furnace is capable of producing 8.7 MW of heat with an efficiency of 92%. In this paper, the numerically obtained heating output of the furnace amounts to about 6.2 MW, which returns an efficiency of 66%. This is because the calculations include only the heat fluxes onto the radiant and convection section while the effects of waste heat recovery are disregarded since not being the subject of this study. Nevertheless, it can be assumed that an economizer installed in the chimney duct can lower the gas temperatures by 500 K. Taking into account that the combustion gases have a flow rate of 14150 kg/h and a heat capacity of 1.2 kJ/kg K, the economizer recovers an additional 2.4 MW of heat. This would bring the total heating output of the furnace to 8.6 MW and its efficiency to 91%, close to the values stated by the refinery. In this case an economizer would increase the efficiency by 25%, whereas values between 10% and 50% have been reported for industrial furnaces [21]. Three swirling burners are placed at the furnace bottom. The burners are radially shifted by 120° from each other and at a distance of 0.8 m from the furnace axis, as shown in Fig. 1. The burners use Y-type steam atomizers with double coaxial tube arrangement. Steam flows inside the central tube and fuel oil flows inside the annular tube. Steam and oil mix inside spray holes drilled inside the atomizer tip. Each atomizer has six uniformly distributed spray holes which spray the steam-oil mist inside the furnace. The steam temperature and pressure are higher than the oil temperature and pressure. Fuel oil is supplied at a temperature of 110 °C and at a pressure of 6 bar while the (superheated) steam is supplied at a temperature of 350 °C and a pressure of 7.5 bar. The steam consumption amounts to 8% of the fuel oil consumption. Combustion air is divided into two streams: primary air which flows coaxially to the burner gun and leaves through the flame-stabilizing impeller, and secondary air which flows through the swirl-generating vanes. The atomizing fluid inlet velocity is 25 m/s and the inlet velocity of the secondary air is 10 m/s.

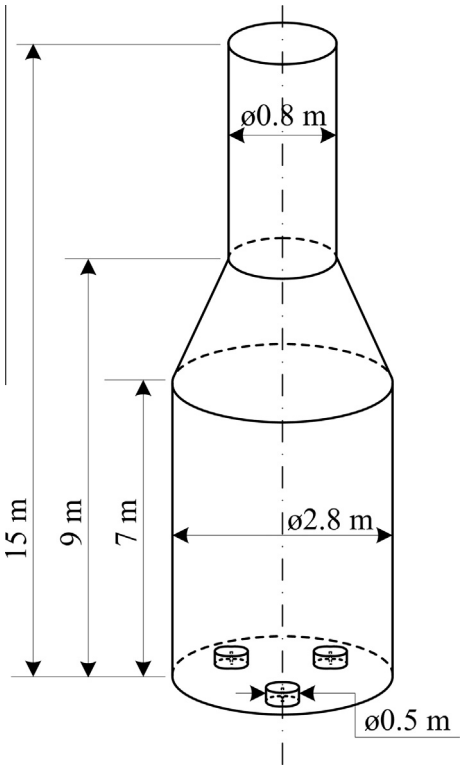

Fig. 1. Scheme of the industrial furnace.

3.2. Fuel oil properties

Heavy fuel oil enters the furnace with mass flow rate of 837 kg/h, temperature of 383 K and pressure of 6 bar. The stoichiometric air mass flow rate is 11 580 kg/h. Air is preheated to 453 K before entering the burners. The physical properties and composition of heavy fuel oil are reported in Table 1.

3.3. Computational domain and boundary conditions

The computational domain is identified as the sector comprising one-third of the furnace on which sides rotational periodicity is applied, as shown in Fig. 2. The boundary conditions are explained next. The computational domain contains one burner with fuel mass flow rate of 279 kg/h whereas the stoichiometric air mass flow rate is 3860 kg/h. The inlet temperatures are 383 K for fuel oil and 453 K for air. The burner swirl number is varied from 0.15 to 1.10. Constant temperature boundary conditions are prescribed to the furnace internal walls: 800 K at the furnace base, 850 K to the walls in the radiant section, 650 K to the walls in the conical section and 550 K in the chimney duct. All surfaces are opaque to heat radiation and have an emissivity of 0.8. Fuel oil droplets are reflected from the furnace surfaces if collision occurs. A cone type injection is used to describe the spray shape from the atomizing nozzles. The domain outlet is defined with the pressure outlet boundary condition. The mesh size sensitivity with regard to the obtained values of furnace heating output and gases tempera-

Table 1
Heavy fuel oil physical properties and chemical composition.

Physical properties		Chemical composition	
Density (288 K), kg/m^3	982.6	Carbon, wt%	88.26
Thermal conductivity (383 K), W/m K	0.1155	Hydrogen, wt%	10.62
Kinematic viscosity (383 K), m^2/s	$21 \cdot 10^{-6}$	Sulfur, wt%	0.84
Diffusion coefficient, m^2/s	$3.79 \cdot 10^{-6}$	Nitrogen, wt%	0.28
Latent heat of vaporization, kJ/kg	211.65		
Lower heating value (LHV), MJ/kg	40.68		
Higher heating value (HHV), MJ/kg	43.01		

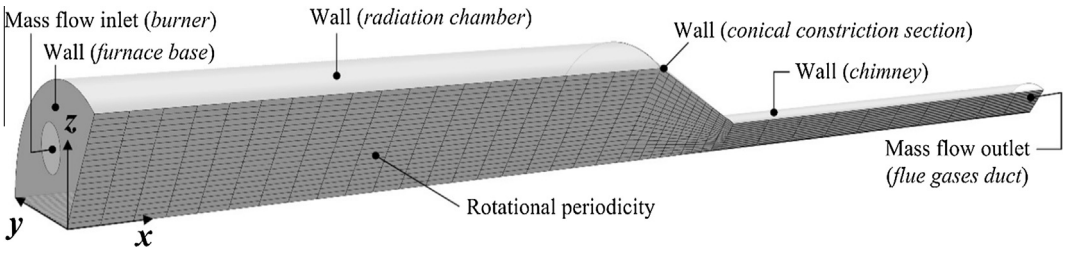

Fig. 2. Computational domain and boundary conditions.

ture at the outlet is shown in Fig. 3. It can be seen that a mesh size of 700,000 rectangular finite volumes represents a good compromise between results accuracy and computer processing time.

4. Results and discussion

4.1. Validation of the combustion model

The combustion model is validated against measurements available for heavy fuel oil spray combustion inside a cylindrical laboratory furnace [10]. The laboratory furnace consists of eight water-cooled steel segments each 0.3 m in height and 0.6 m in internal diameter. The furnace is down-fired to facilitate particulate removal. The burner uses a plain-jet air atomizer with a conventional double coaxial tube arrangement and terminates in a refractory quarl. The burner gun supplies fuel oil through the central tube and compressed air through the annular tube. The burner gun is equipped with tubes for water cooling. The secondary air flows through a moveable-block swirl generator. The measurements on the laboratory furnace consist of O_2, CO_2 and NO fractions taken along the furnace radius and for three distances from the furnace bottom (x = 20, 320 and 620 mm). The turbulent flow in the cylindrical furnace is approached with the axisymmetric swirl model. Three turbulence models are used to describe the highly swirling reacting flow: SKE, RKE and RSM. The comparison between predicted and measured CO_2, O_2 and NO fractions is shown in Figs. 4–6.

In Fig. 4 it can be seen that the RSM model offers good predictions of CO_2 molar fractions in the near-burner region (x = 20 mm), except in the vicinity of the furnace axis. For x = 320 mm, all the three turbulence models overpredict CO_2 concentrations. Better accordance is achieved with the RSM model, though. In Fig. 5, O_2 molar fractions are underpredicted by the SKE and RKE models in the near-burner region (x = 20 mm). On the other side, the RSM model shows very good agreement with measurements. For x = 320 mm, the SKE and RKE models predict constant O_2 fractions along the radial distance while measured values show a growing trend for increasing radial distance. The O_2 fractions predicted by the RSM model show better agreement with measured values. The comparison between predicted and measured molar fractions of NO is shown in Fig. 6. Again, the RSM model gives appreciable improvements over the results of the SKE and RKE models.

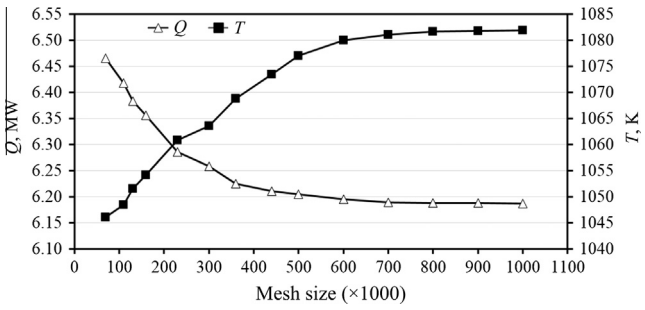

Fig. 3. Mesh sensitivity with regard to furnace heating output (Q) and gases temperature (T).

From the comparison, it can be deduced that the RSM model offers better results than k-ε based models in highly swirling turbulent flows. This is the case for the cylindrical laboratory furnace since the swirl number is S = 1.1. Discrepancies between predicted and measured fractions are found in the near-burner region (x = 20 mm) and about the furnace axis (radial distances under 100 mm). These differences are caused by difficulties in modeling the penetration of the fuel oil jet inside the swirl-generated recirculation zone in front of the burner. Results for x = 620 mm are not shown here, but the predictions of the RSM model are again superior to those of the SKE and RKE models.

The industrial furnace and the laboratory furnace, which was used for model validation, have comparable dimensionless numbers. The Reynolds number for the continuous phase is 50,000 in the laboratory furnace and 61,000 in the industrial furnace, both indicating turbulent flow. These values are reflecting the maximum Reynolds numbers, achieved by secondary swirl air at the inlet. In both furnaces, the temperature and velocity distributions are severely nonuniform. Consequently, the Reynolds number covers a wide range of values, all of which are in the turbulent flow region, justifying the use of the abovementioned turbulence models. The physical properties of the discrete and continuous phases are also similar since both furnaces burn heavy fuel oil and achieve comparable temperatures. Therefore, the Prandtl (≈0.70) and the Schmidt (≈60) numbers are also comparable. The droplet Reynolds number (Eq. (17)) is 2 in the laboratory furnace (mean droplet diameter of 28 μm, injection velocity of 35 m/s, gas velocity of 19 m/s) and 7 in the industrial furnace (mean droplet diameter of 100 μm, injection velocity 25 m/s, gas velocity 10 m/s). The droplet Reynolds number decrease as fuel droplets decelerate and evaporate after the injections. The droplet Reynolds number is zero (Eq. (17)) when the droplet velocity is equal to the gas velocity. Thus, the droplet Nusselt number (Eq. (15)) is between 2 and 2.8 in the laboratory furnace, and between 2 and 3.4 in the industrial furnace. The droplet Sherwood number (Eq. (16)) is between 2 and 5.3 in the laboratory furnace, and between 2 and 8.1 in the industrial furnace. The above dimensionless numbers are comparable and the chosen combustion model can be used for numerical analysis of the industrial furnace.

4.2. Results for the industrial furnace

4.2.1. Effect of air-fuel ratio

Reported here are the results obtained for seven values of relative air-fuel ratio (*AFR*): 0.9, 0.975, 1.05, 1.125, 1.15, 1.20 and 1.275. The following parameters have fixed values: the droplet diameter (d_p) is 50 μm, the fuel spray half-angle (φ) is 42.5° and the swirl number (S) is 0.78. The furnace heating output (Q) and flue gases temperatures (T) are shown in Fig. 7. The highest heating output

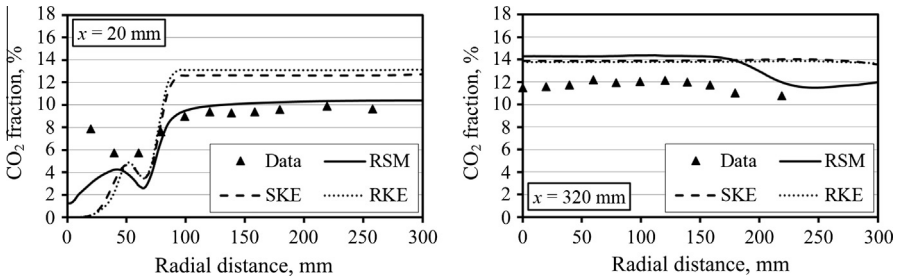

Fig. 4. Comparison between predicted and measured [10] molar fractions of CO_2.

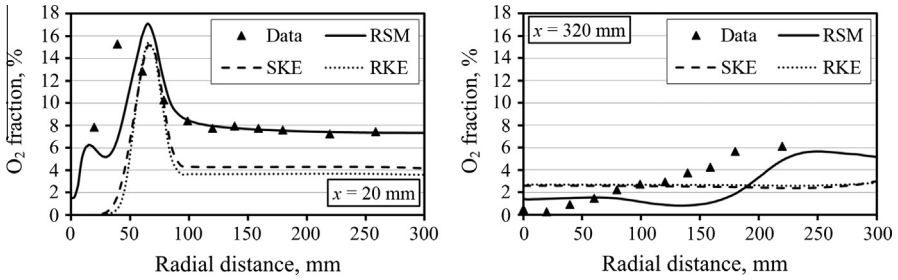

Fig. 5. Comparison between predicted and measured [10] molar fractions of O_2.

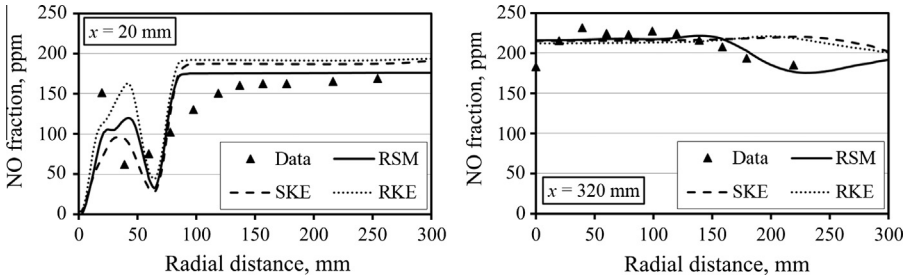

Fig. 6. Comparison between predicted and measured [10] molar fractions of NO.

and flue gases temperature are achieved for near-stoichiometry conditions that is for *AFR* values between 0.95 and 1.05. Larger *AFR* values return lower heating outputs and gases temperatures because of larger quantities of air and higher sensible heat losses. CO, H_2, NO and SOx molar fractions at the furnace outlet are given with Fig. 8. For *AFR* = 0.9, the molar fractions of unburnt species CO and H_2 are 17‰ and 13‰, and decrease rapidly, down to 0‰ for *AFR* = 1.15. This is expected since lower *AFR* values promote incomplete combustion that results in higher fractions of unburnt species.

SOx and NO fractions decrease with the *AFR* value because of the relatively larger quantity of air in flue gases. The SOx fraction

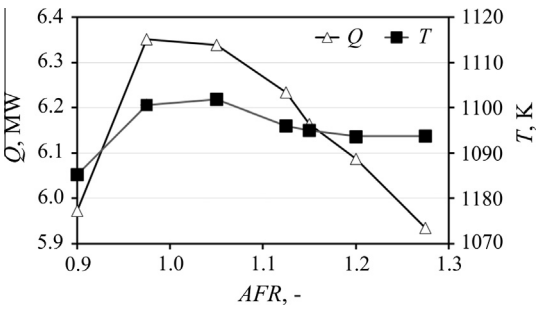

Fig. 7. Heating output and gases temperature vs *AFR* number.

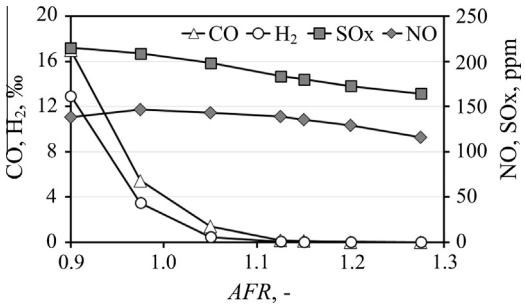

Fig. 8. Molar fractions of CO, H_2, NO and SOx vs *AFR* number.

(SO_2 and SO_3) is 215 ppm at *AFR* = 0.90 and decreases to 165 ppm for *AFR* = 1.275. It should be noted that SO_3 accounts for only 1% of the total SOx emission in this case. Typically, between 1% and 3% of sulfur is converted into SO_3 during combustion of heavy fuel oil [22]. On the other side, NO fractions are in the range of 115–145 ppm where the maximum occurs at *AFR* = 1.0. Fuel and thermal NO are found to be the largest contributors to NO emissions, with 90% and 10%, respectively. The contribution of prompt NO is negligible.

4.2.2. Effect of fuel spray half-angle

The atomizing nozzle ejects fuel oil droplets into a hollow cone shaped spray. Seven different fuel spray half-angles are considered

here: 20°, 30°, 40°, 47.5°, 55°, 62.5° and 70°. The following parameters have fixed values: $AFR = 1.15$, $d_p = 75$ μm and $S = 0.78$. The effect of fuel spray half-angle on the furnace heating output (Q) and flue gases temperatures (T) is shown in Fig. 9. It can be seen that larger spray half-angles reduce the furnace heating output and flue gases temperature as well. This is explained next. Narrow spray angles deteriorate the mixing between air and fuel droplets. As a consequence, fuel droplets ignite later and the flame region is elongated. This results with more favorable distribution of temperatures inside the furnace and higher heat fluxes onto the radiant and convection section. On the other hand, large spray angles enhance mixing between air and fuel droplets, which ignite faster and closer to the burners. Now, the flame region is attached to the furnace base and the furnace heating output is reduced, as shown in Fig. 9. Combustion with large spray angles cause flame shortening and unfavorable distribution of heat fluxes on the furnace walls. It should be noted, however, that the global energy output of the furnace increases for larger spray angles. This is due to better mixing between fuel and air, and lower fractions of unburnt species at the furnace outlet. This is not seen in Fig. 9 because the furnace heating output includes only the heat fluxes on the radiant and convection sections. If the furnace base was accounted for in the calculations, the furnace heating output would increase along with the spray angle. The fractions of SOx pollutants, CO and H_2 unburnt species are reduced for larger spray angles, as shown in Fig. 10, which is a consequence of enhanced mixing between fuel and air. NO fractions exhibit little variation with the spray half-angle, though.

4.2.3. Influence of fuel oil droplet diameter

The size of the fuel oil droplets depends on the pressure in the atomizing nozzle. The size of fuel oil droplets influences the fuel penetration pattern through the recirculation zone, and consequently the flame geometry and stability. Generally, in liquid sprays, larger fuel droplets follow ballistic trajectories and their motion is influenced by the initial nozzle characteristics rather than by the surrounding gas phase [23]. On the other side, smaller droplets are more influenced by the gas phase because they lose their inertia quickly. Also, smaller droplets mix better with the gas phase, evaporate and ignite earlier than larger droplets. In this study, the droplet size distribution is described with the Rosin-Rammler function, which is defined by the mean droplet diameter and the spread parameter. The spread parameter is 1.4 and the continuous droplet size distribution is approximated by 20 discrete droplet sizes. Results are shown for seven mean diameters: 25, 50, 75, 100, 125, 150 and 175 μm, while the following parameters have fixed values: $AFR = 1.15$, $\varphi = 42.5°$ and $S = 0.78$. The effect of droplet diameter on the furnace heating output and flue gases temperature is shown with Fig. 11. Small droplets achieve high heating outputs and gas temperatures. This is because the vaporization and the mixing between air and fuel are enhanced by small droplets. On the other side, large fuel oil droplets are more prone to incomplete combustion because they need more time to evaporate and

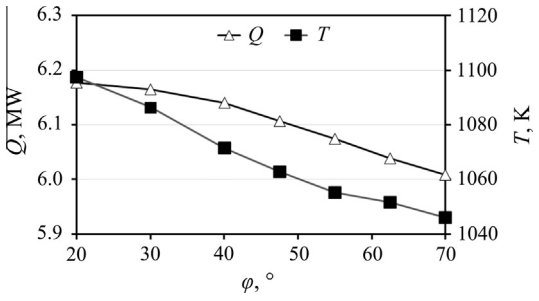

Fig. 9. Heating output and gases temperature vs fuel spray half-angle.

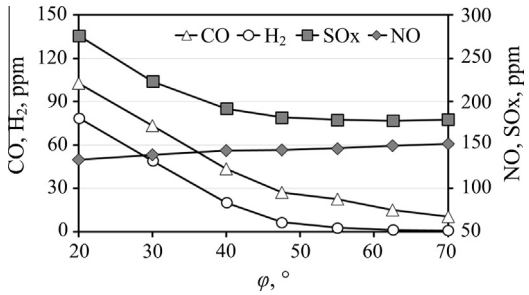

Fig. 10. Molar fractions of CO, H_2, NO and SOx vs fuel spray half-angle.

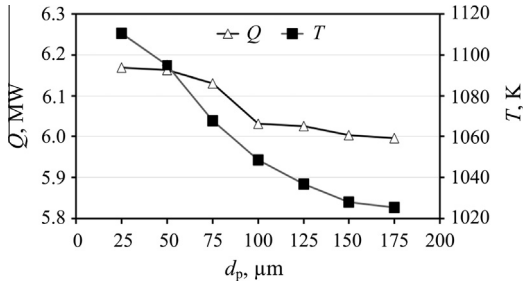

Fig. 11. Heating output and gases temperature vs mean droplet diameter.

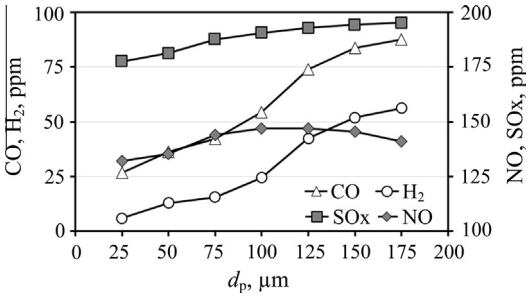

Fig. 12. Molar fractions of CO, H_2, NO and SOx vs mean droplet diameter.

ignite. Consequently, CO and H_2 fractions increase, as shown in Fig. 12. SOx fractions increase slightly while NO fractions show no general trend with the droplet diameter.

4.2.4. Influence of burner swirl number

Compared to nonswirling burners, swirl burners have the ability to improve the combustion efficiency and to reduce the emission of pollutants. Here, the analysis includes results for seven swirl numbers: 0.15, 0.30, 0.42, 0.60, 0.78, 0.93 and 1.10. The swirl number is defined as the ratio of the angular momentum flux to the axial momentum flux, that is

$$S = \frac{\int_{R_i}^{R_o} w_a w_t r^2 dr}{\int_{R_i}^{R_o} w_a^2 r dr} \tag{23}$$

The hub radius and the outer radius of the swirl generator are R_i and R_o, respectively. The tangential flow component is denoted with w_t and the axial flow component with w_a. The parameters with fixed values are: $AFR = 1.15$, $\varphi = 42.5°$ and $d_p = 100$ μm. From Fig. 13 it can be seen that low swirl flows ($S < 0.4$) delay ignition, produce elongated flames and cause increased concentrations of unburnt species. The elongated flame shape push large quantities of heat directly into the chimney which in turn causes higher gas temperatures at the outlet and lower heating outputs. High swirl

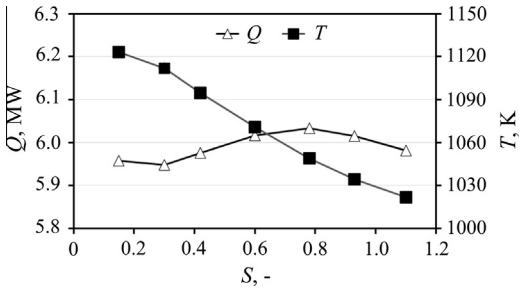

Fig. 13. Heating output and gases temperature vs burner swirl number.

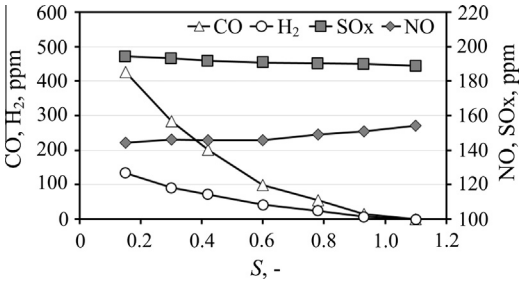

Fig. 14. Molar fractions of CO, H_2, NO and SOx vs burner swirl number.

flows ($S > 0.6$), on the other hand, strengthen the recirculation zone in front of the burners and generate shorter but wider flame regions. Consequently, the gas temperatures at the outlet is reduced and the furnace heating output is increased, as shown in Fig. 13. The highest heating outputs are achieved for swirl numbers between 0.6 and 1.0, with the peak value at 0.78. Swirl numbers above 1.0 do not bring further increases in the heating output, most likely because the short flame region results with unfavorable temperature distributions inside the furnace and reduced heat fluxes towards the furnace walls. The fractions of unburnt species CO and H_2 decrease with the swirl number, as shown in Fig. 14. This is expected since high swirl numbers enhance mixing between fuel and air. On the other side, pollutant fractions of SOx and NO show no decisive trends: NO is slightly increased and SOx is slightly decreased with the burner swirl number.

4.3. Solution of flow fields

The effect of *AFR* value on CO fractions for fuel oil spray combustion inside the industrial furnace is shown in Fig. 15. Results are given for *AFR* values of 0.90, 1.05 and 1.20, and for three cross sections from the furnace base, that is, for $x = 1$ m, 2 m and 3 m. It can be seen that CO fractions decrease with the increase of *AFR* value. Similar is the effect of the fuel spray angle. In Fig. 16 results are given for three fuel spray half-angles: $\varphi = 30°$, 42.5° and 67.5°. Wide fuel spray angles expand the flame region and improve the

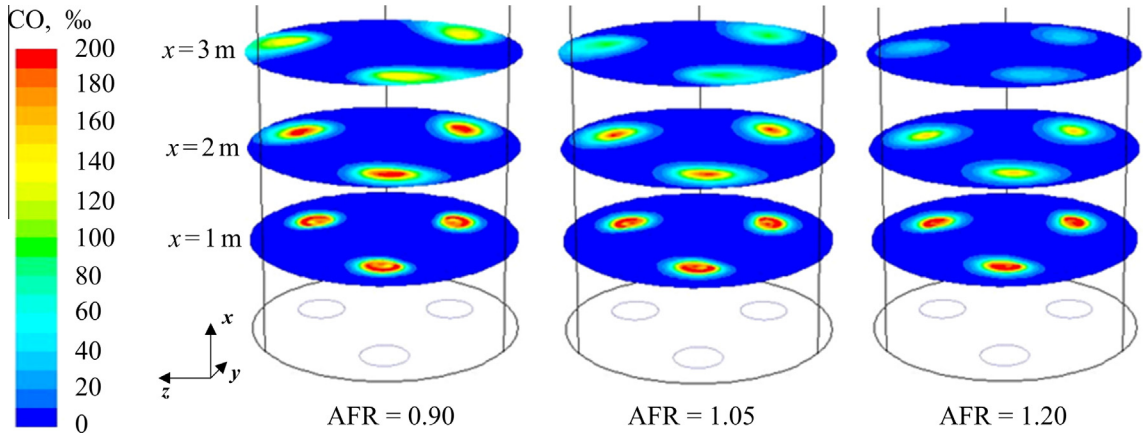

Fig. 15. CO fractions for *AFR*: 0.90, 1.05 and 1.20, fixed values: $d_p = 50$ μm, $\varphi = 42.5°$, $S = 0.78$.

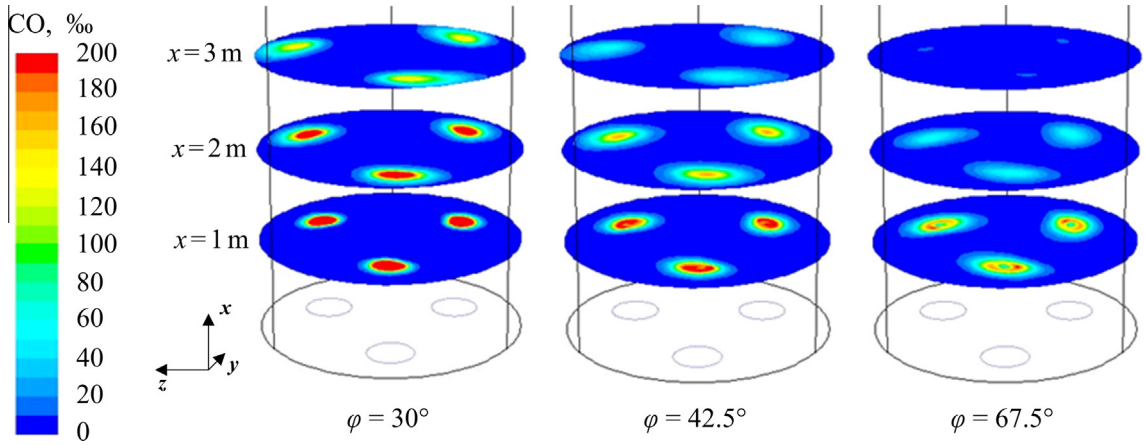

Fig. 16. CO fractions for φ: 30°, 42.5° and 67.5°, fixed values: *AFR* = 1.15, $d_p = 50$ μm, $S = 0.78$.

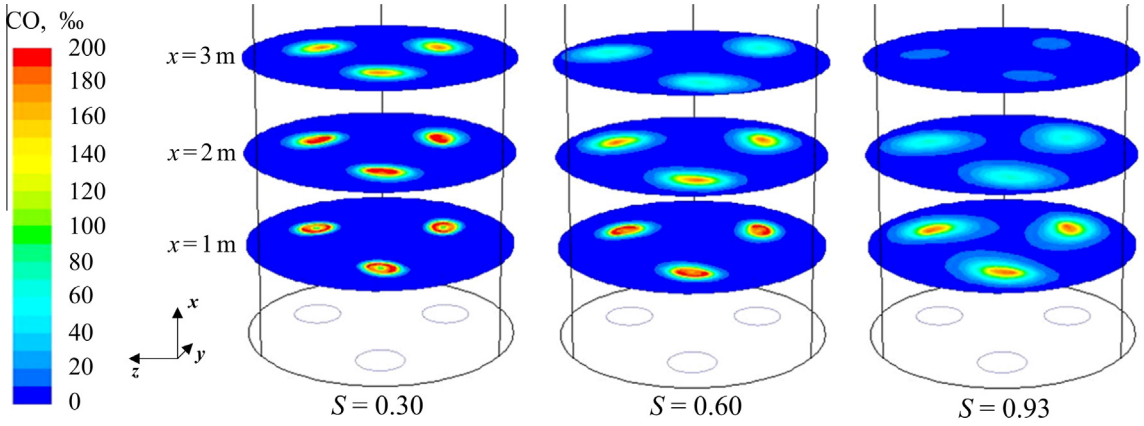

Fig. 17. CO fractions for S: 0.30, 0.60 and 0.93, fixed values: AFR = 1.15, d_p = 50 μm, φ = 42.5°.

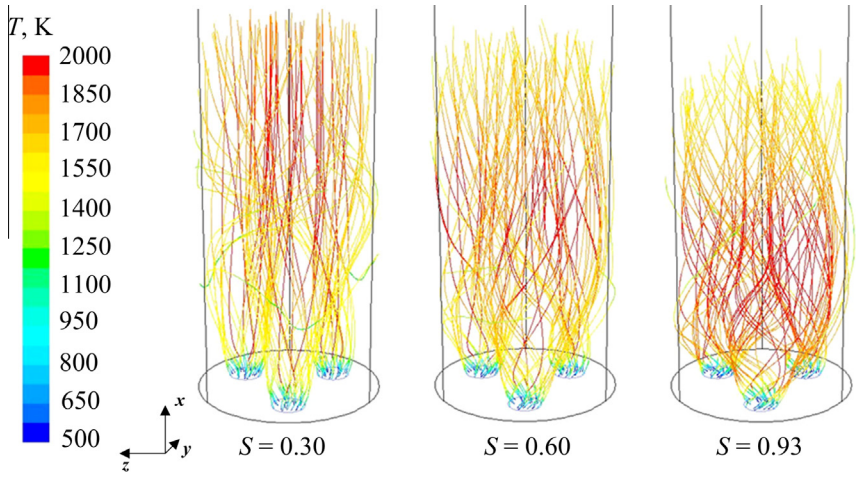

Fig. 18. Flow pathlines for burner swirl numbers S: 0.30, 0.60 and 0.93.

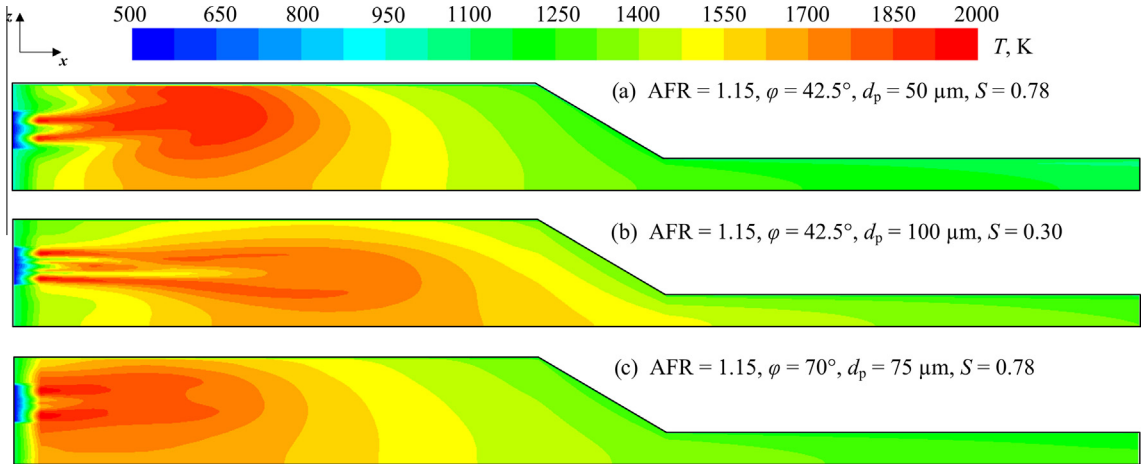

Fig. 19. Temperature distributions for three burner setups.

mixing between air and fuel. Consequently, unburnt species fractions are decreased while the furnace heating output is increased.

The fractions of unburnt species can be reduced by increasing the burner swirl number, as shown in Fig. 17. The distribution of CO fractions are given for three swirl numbers: S = 0.30, 0.60 and 0.93. Spray combustion with high swirls is featured by strong flow recirculation in front of the burners. This swirl stabilization results with a shortened flame region, as it can be seen from Fig. 18. Low swirling burners disperse fuel droplets farther downstream, which originates elongated flames. Consequently, the unburnt species fractions are increased and the furnace heating output is decreased. On the other hand, high swirling burners enhance the mixing between fuel and air by promoting radial dispersion and spatial uniformity of fuel droplets in the near-burner region [23].

Fig. 19 shows the temperature distributions and flame shapes in the plane of the burner axis, for fuel oil spray combustion with three different burner setups. It can be seen that small swirl number and large oil droplets produce elongated flames (Fig. 19b). Highly swirling burners generate shorter flames and increase the heating output (Fig. 19a). Among the three setups, the highest heating output of 6.16 MW is achieved with a swirl number of 0.78 and mean droplet size of 50 μm (Fig. 19a). The lowest heating output of 5.95 MW is obtained with a swirl number of 0.30 and mean droplet diameter of 100 μm (Fig. 19b). This burner setup results also with higher emissions of pollutants: 26% more NO emissions and 7% more SOx emission, relatively to the emissions of the first burner setup. The third burner setup (Fig. 19c) exhibits a wide flame region because of the large fuel spray angle. The resulting heating output is 6 MW.

5. Conclusions

In this paper, fuel oil spray combustion in an industrial furnace has been studied numerically. The predictions of the non-premixed combustion model together with three different turbulence models have been tested against measurement data found in the literature. It was found that the RSM turbulence model gives better predictions than k-ε based models for the highly swirling turbulent flow in the industrial furnace.

The effects of fuel and burner parameters such as air-fuel ratio, fuel droplet size, burner swirl number and fuel spray angle on the quality of the combustion process have been analysed. Regarding the influence of the *AFR* value, it was found that *AFR*s larger than 1.15 ensure complete combustion and minimum fractions of unburnt species CO and H_2. The fractions of pollutants NO and SOx also decrease with the *AFR* value, but this is because of the relatively larger quantity of air in flue gases. However, the highest furnace heating output is achieved for near-stoichiometric conditions, that is, for *AFR* values around 1.0. For the analysed heavy fuel oil composition, it was found that SO_2 emissions contribute with 99% while SO_3 emissions contribute with 1% in the total SOx emissions. On the other hand, NO emissions consist of 90% fuel NO and 10% thermal NO while prompt NO is negligible.

The fuel spray half-angle has similar effects on the furnace heating output and species emission. Wide spray half-angles promote the spatial dispersion of fuel droplets in the near-burner region. The flame region is wider but shorter and the average particle residence time is prolonged. Consequently, CO and H_2 emissions as well as SOx fractions are reduced significantly for spray half-angles above 50°. However, the heating output is also decreased because short flames negatively affect the distribution of heat fluxes towards the furnace walls. The numerical analysis revealed that mean droplet diameters under 100 μm ensure high heating outputs and low pollutant emissions. Larger fuel droplets need more time to evaporate and burn, which makes them more prone to incomplete combustion.

The burner swirl number has a major effect on the shape of the flame and on the mixing rate between air and fuel. Increasing the swirl number ensures better mixing between fuel and air and improved spatial uniformity of fuel droplets in the near-burner region. Hence, the fractions of unburnt species CO and H_2 decrease with the swirl number. On the other hand, the furnace heating output does not increase linearly with the swirl number. The maximum heating output is achieved for swirl numbers around 0.8 while swirls above 1.0 reduce the heating output because of excessive flame shortening.

Acknowledgements

This research has been performed as part of the scientific project Research and Development of Renewable Energy Components and Systems (grant number: 069-0692972-3112), supported by the Ministry of Science, Education and Sports of the Republic of Croatia.

References

[1] International Energy Agency, World Energy Outlook 2015, OECD/IEA, IEA Publications, Paris, France, 2015.
[2] I. Bonefačić, B. Franković, A. Kazagić, Cylindrical particle modelling in pulverized coal and biomass co-firing, Appl. Therm. Eng. 78 (2015) 74–81.
[3] S. Nemoda, V. Bakić, S. Oka, G. Zivković, N. Crnomarković, Experimental and numerical investigation of gaseous fuel combustion in swirl chamber, Int. J. Heat Mass Transf. 48 (2005) 4623–4632.
[4] L.M. Gicquel, G. Staffelbach, T. Poinsot, Large eddy simulations of gaseous flames in gas turbine combustion chambers, Prog. Energy Combust. 38 (2012) 782–817.
[5] D.R. Schneider, Ž. Bogdan, Effect of heavy fuel oil/natural gas co-combustion on pollutant generation in retrofitted power plant, Appl. Therm. Eng. 27 (2007) 1944–1950.
[6] A. Maghbouli, T. Lucchini, G. D'Errico, A. Onorati, Effects of grid alignment on modeling the spray and mixing process in direct injection diesel engines under non-reacting operating conditions, Appl. Therm. Eng. 91 (2015) 901–912.
[7] P. Jenny, D. Roekaerts, N. Beishuizen, Modeling of turbulent dilute spray combustion, Prog. Energy Combust. 38 (2012) 846–887.
[8] H. Chiu, Advances and challenges in droplet and spray combustion: toward a unified theory of droplet aerothermochemistry, Prog. Energy Combust. 26 (2000) 381–416.
[9] W.A. Sirignano, Advances in droplet array combustion theory and modeling, Prog. Energy Combust. 42 (2014) 54–86.
[10] A. Saario, A. Rebola, P.J. Coelho, M. Costa, A. Oksanen, Heavy fuel oil combustion in a cylindrical laboratory furnace: measurements and modelling, Fuel 84 (2005) 359–369.
[11] A. Barreiros, M.G. Carvalho, M. Costa, F.C. Lockwood, Prediction of the near burner region and measurements of NOx and particulate emissions in heavy fuel oil spray flames, Combust. Flame 92 (1993) 231–240.
[12] Z. Ling, X. Zeng, T. Ren, H. Xu, Establishing a low-NOx and high-burnout performance in a large-scale, deep-air-staging laboratory furnace fired by a heavy-oil swirl burner, Appl. Therm. Eng. 79 (2015) 117–123.
[13] S.R. Wu, W.C. Chang, J. Chiao, Low NOx heavy fuel oil combustion with high temperature air, Fuel 86 (2007) 820–828.
[14] H.K. Versteeg, W. Malalasekera, An Introduction to Computational Fluid Dynamics: The Finite Volume Method, second ed., Pearson Education, Essex, 2007.
[15] W.E. Ranz, W.R. Marshall, Evaporation from drops, part I and part II, Chem. Eng. Prog. 48 (1952) 173–180.
[16] D.G. Sloan, P.J. Smith, L.D. Smoot, Modelling of swirl in turbulent flow systems, Prog. Energy Combust. 12 (1986) 163–250.
[17] P.A. Tesner, T.D. Snegiriova, V.G. Knorre, Kinetics of dispersed carbon formation, Combust. Flame 17 (1971) 253–260.
[18] B.F. Magnussen, B.H. Hjertager, On mathematical models of turbulent combustion with special emphasis on soot formation and combustion, in: 16th International Symposium on Combustion, The Combustion Institute, 1976.
[19] I. Glassman, R.A. Yetter, Combustion, fourth ed., Academic Press, San Diego, 2008.
[20] J.C. Kramlich, The fate and behavior of fuel-sulfur in combustion systems PhD thesis, Washington State University, Washington, 1980.
[21] US Department of Energy, Waste Heat Recovery: Technology and Opportunities in U.S. Industry, Industrial Technologies Program, 2008. <http://www1.eere.energy.gov/manufacturing/intensiveprocesses/pdfs/waste_heat_recovery.pdf> (accessed 10.08.16).
[22] D.R. Schneider, Ž. Bogdan, Modelling of SO_3 formation in the flame of a heavy-oil fired furnace, Chem. Biochem. Eng. Q. 17 (2003) 175–181.
[23] C. Presser, C.T. Avedisian, J.T. Hodges, A.K. Gupta, Behavior of droplets in pressure-atomized fuel sprays with coflowing air swirl, in: K. Kuo (Ed.), Recent advances in spray combustion: spray combustion measurements and model simulation, vol. II, American Institute of Aeronautics and Astronautics, Reston, USA, 1996, pp. 31–61.